# Memristor-Based CNNs for Detecting Stress Using Brain Imaging Signals

SuJin Bak, Jinwoo Park, Jaehoon Lee, and Jichai Jeong, *Senior Member, IEEE*

***Abstract*—Typical convolutional neural networks (CNNs) are widely used to recognize a user's stress state using the functional near-infrared spectroscopy (fNIRS), which is the latest brain imaging technology. fNIRS signals are usually fed into CNN models in the form of high-dimensional image data. However, this approach is not easy to achieve high classification accuracy because of physiological noises in brain signals. It is also likely to overlook the process of evaluating the reliability of calculated classification accuracy. To solve these problems, we proposed a memristor-based CNN (M-CNNs) This model's weight update process involves using stochastic gradient descent with momentum (SGDM), where the normalized conductances of memristors are used as weight substitutes. These conductances are then adjusted to classify stress states. We calculated the classification accuracies between the control and stress groups by using the M-CNNs, and then compared them with those of the CNNs. We used DenseNet, the most recent CNN model, to simulate accuracy under the same conditions. To ensure a fair comparison, we divided the DenseNet into the memristor-based DenseNet (M-DenseNet) and the conventional DenseNet (C-DenseNet). As a result, we discovered that the accuracy of M-CNNs (93.33%) exceeded that of CNNs (87.50%), and is reliable by precision, recall, and F-Score calculated from a confusion matrix. Likewise, M-DenseNet (92.38%) has higher accuracy than C-DenseNet (90.00%), but shows lower accuracy than M-CNNs. Moreover, we observed the reproducibility of M-CNN/DenseNet in various datasets. Therefore, our study suggests a promising application of CNN by combining conductances of memristor for classifying stress states.**

***Index Terms*—Convolutional neural networks (CNNs), DenseNet, functional near-infrared spectroscopy (fNIRS), memristor, stress detection.**

## I. Introduction

VON Neumann architecture has been a mainstay of modern computers and electronics industries for several decades [1]. This architecture, however, is still facing many challenges, such as power budget, delay, and scalability [2]. To address these problems, many researchers have developed a variety of neuromorphic hardware including non-volatile memories, such as phase-change memory [3], resistance change memory [4], and conductive bridge memory [5] for storage and computing integration. These kinds of memories are called memristors, and they imitate the principles of biological synapses in a huge network of neurons [6]. Memristor devices have emerged as a promising way to implement extremely energy-efficient, time-efficient, and fault-tolerant computing technologies [7].

These memristors are mainly used in neural network models based on deep learning [8], [9]. Memristors are good at parallel processing, which facilitates a convolution operation such as feature extractions in the convolutional neural networks (CNNs) model [10]. Moreover, memristors can construct arrays as convolutional kernels of CNN [11]. Thus, recent studies have proposed a novel approach to the CNN architecture composed of memristor crossbar arrays [8]. Unlike the approach of CNN combined with memristors, the conventional CNNs model has made significant contributions to classifying and diagnosing stress states. The word "stress" always attracts many people's attention because it is routinely experienced by many in today's complex society [12]. Research on stress is important because it affects an individual's health and performance such as daily output and task accuracy [13]. Ruiqi, F. et al. [14] obtained an accuracy of 87.62% to classify stress states based on brain signals. Another study developed a CNN model that determines emergency braking detection for stressed drivers, resulting in 71.8% detection [15]. However, these novel studies still have significant potentials for improving the detection of stress states. For improving the performances, we believe that memristors are capable of mimicking typical human synaptic functions such as synapse plasticity [16], learning [17], and forgetting [18], and therefore memristor based neural networks can be an alternative.

Therefore, in our study, we decided to use our previously collected stress-dataset [19] along with CNN models that transformed the memristor's conductances into weights of neural

Manuscript received 21 December 2022; revised 10 April 2023; accepted 22 June 2023. Date of publication 28 July 2023; date of current version 23 January 2024. This work was supported in part by the Korea Agency for Infrastructure Technology Advancement (KAIA) grant funded by the Ministry of Land, Infrastructure and Transport under Grant 20LTSM-B156015-01 and in part by the Institute of Information and Communications Technology Planning & Evaluation funded by the Korea Government (MSIT), Development of BCI based Brain and Cognitive Computing Technology for Recognizing User's Intentions using Deep Learning, under Grant 2017-0-00451. Recommended for acceptance by Albert Lam. *(SuJin Bak and Jinwoo Park are co-first authors.) (Corresponding authors: Jaehoon Lee; Jichai Jeong.)*

This work involved human subjects or animals in its research. Approval of all ethical and experimental procedures and protocols was granted by Institutional Review Board of Korea University under Application No. KUIRB-2020-0061-01, and performed in line with the Declaration of Helsinki.

SuJin Bak is with the Advanced Institute of Convergence Technology, Suwon-si 16229, Republic of Korea (e-mail: soojin7897@snu.ac.kr).

Jinwoo Park is with the Department of Artificial Intelligence, Korea University, Seoul 02841, Republic of Korea (e-mail: pjinwoo123@korea.ac.kr).

Jaehoon Lee is with the Department of Computer Science and Engineering, Korea University, Seoul 02841, Republic of Korea (e-mail: ejhoon@korea.ac.kr).

Jichai Jeong is with the Department of Brain and Cognitive Engineering, Korea University, Seoul 02841, Republic of Korea (e-mail: jcj@korea.ac.kr).

Digital Object Identifier 10.1109/TETCI.2023.3297841

networks. It is anticipated that this strategy will increase the classification accuracy between control and stress groups.

To measure hemoglobin responses to stress, we introduce the functional near-infrared spectroscopy (fNIRS), which is a state-of-the-art neuroimaging technique [20]. Although functional magnetic resonance imaging (fMRI) is mainly used as a technology for in vivo imaging of the human brain, it is inappropriate in standard laboratory environments because of electromagnetic compatibility constraints, high sensitivity to motion artifacts, and high cost [21]. However, the fNIRS stands out for its portability and safety, because it allows functional imaging to be used in much more realistic settings [21]. The fNIRS also has a much higher temporal resolution than the fMRI because it allows for the measurements of concentration changes in both oxygenated ($\Delta\mathrm{HbO}$) and deoxygenated ($\Delta\mathrm{HbR}$) hemoglobin [22]. Additionally, hemodynamic responses acquired by fNIRS facilitate stress detection and diagnosis. Recently, other studies found that fNIRS helps detect stress states with the CNNs [23], [24]. A study has reported a classification accuracy of 72.77% between a stress-causing task and stress-free (non-task) using CNNs [25]. Likewise, some studies achieved the classification accuracies between control and stress status within the range of 80–87% [25], [26]. Previous studies, however, still exhibited a lower accuracy, because it is not easy to classify control and stress signals because of the physiological noises in brain signals [27].

In this study, we propose a memristor-based CNN (M-CNN) model by updating the weights according to the memristor's conductances to improve the classification accuracy between the control and stress groups. To assess the accuracies calculated from the M-CNN, we compared them with those of the conventional CNN (CNNs) and verified whether their classification results are reliable. In this study, the memristor-modified CNN is referred to as M-CNNs, while the conventional CNN is referred to as CNNs. To achieve these goals, we chose the publicly available fNIRS-stress datasets generated in our previous study [19] and then converted them into brain imaging signal sets. During neural network learning, the differences in the values between the positive (increased) and negative (decreased) conductance changes in the potentiation process and the depression process are calculated to be used as weights, respectively. Weights are updated by the stochastic gradient descent with momentum (SGDM). We obtained a higher classification accuracy in M-CNNs (93.33%) than in CNNs (87.50%). Furthermore, their classification results were proved to be reliable by calculating a confusion matrix with precision, recall, and F-Score. We used a two-independent sample t-test to verify the statistical significance of the accuracy results calculated from M-CNNs and CNNs. We further compared the proposed model to the DenseNet model, which is the latest neural network model, to ensure a fair and reliable comparison. We divided the DenseNet model into the conventional DenseNet (C-DenseNet) and the memristor-style DenseNet (M-DenseNet) and compared their accuracies with CNNs and M-CNNs. We achieved higher classification accuracy in M-DenseNet (92.38%) than C-DenseNet (90.0%). This result exhibits the same tendency in the results of CNNs. Moreover, M-CNNs show higher accuracy than M-DenseNet. We also demonstrated whether the M-CNNs and M-DenseNet provide the reproducible results using the modified national institute of standards and technology (MNIST) datasets and Merchandise sets (Merch) as well as the fNIRS-stress datasets. We first attempted to classify the stress states using the M-CNNs, which resulted in improved accuracy when compared with the other models. fNIRS datasets have not been used for memristor based CNN models yet. We believe that our findings will be useful in the design and optimization of M-CNNs for classifying stress states.

## II. Materials and Methods

We proposed the M-CNN model to classify control group and stress group based on fNIRS datasets, which has already been recorded in our previous studies [19]. The fNIRS data was stored as two-dimensional brain image data using the fNIRS software analysis tools to compare the performance of M-CNNs and CNNs. To prove the excellence of the proposed model, we compared the classification accuracy of the proposed M-CNN model with that of the existing CNN model. While implementing M-CNN, it is a very important process to convert the memristor's conductances into weights of the neural networks. Weights play an important role in adjusting the input signals to yield correct output signals. We converted the memristor's conductances into weights, and then reflected them to the M-CNN model. We also evaluated the reliability of the calculated accuracy results from the proposed model by using a confusion matrix and analyzed the difference in averaged accuracies by the M-CNN and CNNs using a two-independent sample t-test.

### A. Description of fNIRS Dataset

In this study, we adopted our publicly available fNIRS stress dataset [19], a state-of-the-art dataset for stress analysis. The dataset consists of the hemodynamic responses for the 22 control and 22 stress groups measured from the fNIRS. Fig. 1 illustrates the channel configurations and concepts of generating brain imaging signals from fNIRS signals. The detected light signals in each wavelength (780 and 850 nm) were filtered by a band-pass filter in the range of 0.01–0.1 Hz. The sampling rate of the measured signals was set to 8.138 Hz. The signals were converted to the concentration changes of oxygenated ($\Delta\mathrm{HbO}$) and deoxygenated ($\Delta\mathrm{HbR}$) hemoglobin by using the modified Beer–Lambert law [28]. We focused on $\Delta\mathrm{HbO}$ signals rather than $\Delta\mathrm{HbR}$ because of high hemodynamic activations [29]. The $\Delta\mathrm{HbO}$ signals were segmented into epochs corresponding to one ranging from -1 to 60 s relative to the task onset (i.e., 0 s). Epochs were adjusted to baseline correction by subtracting the average value within the reference interval between -1 and 0 s. As shown in Fig. 1, we finally converted the measured $\Delta\mathrm{HbO}$ signals at the 15 locations in the prefrontal cortex (PFC) region into the two-dimensional brain images (28-by-28 pixels) using the fNIRS software analysis tools, because the neural network models are optimized for image processing and classification [30]. A total of 44 images were obtained from the 22 control groups and 22 stress groups. These images were used as the inputs for the neural network models.

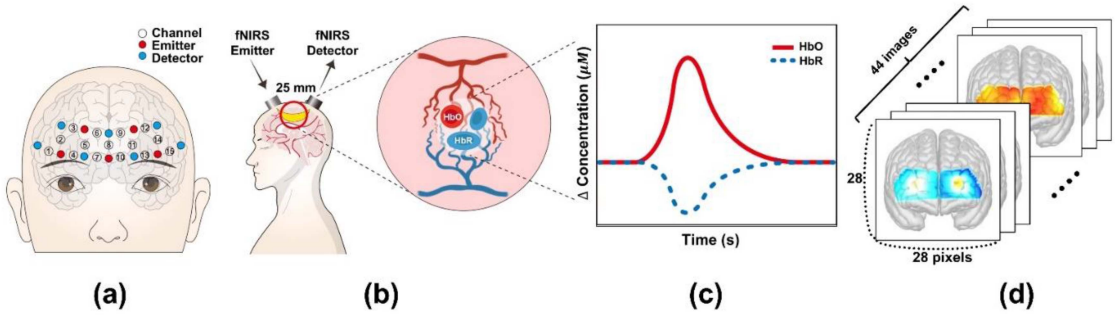


Fig. 1. Schematic of obtaining brain imaging signals from $\Delta$HbO and $\Delta$HbR measured by fNIRS. (a) The overall location of 15 channels (red circles: emitters and blue circles: detectors) at the prefrontal cortex (PFC). The channels are placed on each participant's head at a reference point FPz between channels 7 and 10 according to the 10/20 international system. The distance between the emitter and detector is 25 mm. (b) An example of emitter-detector pair showing a banana-shaped path of light. In this process, we obtain brain hemodynamic signals of HbO and HbR. (c) The hemodynamic response measured from fNIRS. The measured HbO signal is represented by a red line, and the HbR signal is indicated by a blue dotted line. (d) Brain imaging signals converted from hemodynamic responses. The total number of images is 44, which corresponds to 22 images for both the control group and the stress group. The pixel size per image is $28 \times 28$. Therefore, we used publicly available fNIRS-datasets that went through this process, which has already been reported in our previous study. These converted images become the inputs to the neural network models.

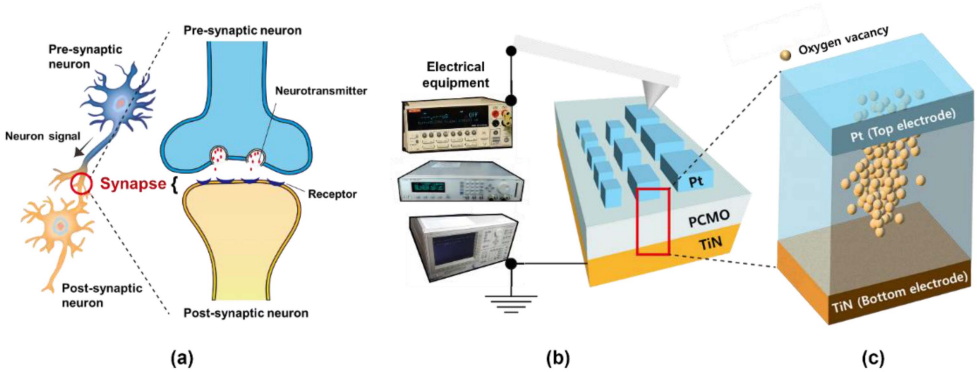


Fig. 2. Memristor as artificial synapse imitating a biological synapse in the human brain system: (a) biological synapse between a pre-synaptic neuron and a post-synaptic neuron. The principle of this bio-synapse is very similar to memristors. (b) Schematic of an electrical measurement method for a three layered memristor using the electrical equipment to determine switching characteristics, such as current-voltage (I-V) characteristics, and (c) structure of enlarged two-terminal $Pr_{0.7}Ca_{0.3}MnO_3$ memristor consisting of switching layer, top electrode (Pt), and bottom electrode (TiN). The balls in the middle layer indicate oxygen vacancies, which form filaments that act as a passage for current flow.

### *B. Description of Memristor Properties*

To convert the memristor's conductances into synaptic weights, we adopted the Pt/$Pr_{0.7}Ca_{0.3}MnO_3$ (PCMO)/TiN memristor devices by Pyo et al. [31]. Before measuring the memristor's conductances, we measured the current-voltage (I-V) curves to study the memristor's resistive switching characteristics by using a source meter (Keithley 2400, Solon, OH, USA). Memristors can have genuine synaptic characteristics with hysteresis shapes of I-V curves [32]. We further repeatedly measured the memristor's conductances by using a semiconductor analyzer (4155C SCS, Keithley, Solon, OH, USA) and a pulse function arbitrary noise generator (Agilent 81110A, Santa Clara, CA, USA). The conductances were increased or decreased depending on the number of P-pulses or D-pulses, respectively. Consecutive P-pulses or D-pulses can be used to achieve continuous tuning of conductances in memristor devices implemented from a three-layer structure of Pt, PCMO, and TiN, as illustrated in Fig. 2. Memristors have similar structure to human biological synapses [33], [34], [35], [36], [37], [38]. These three layered memristors can function as pre-synaptic neuron or post-synaptic neuron within biological neurons [39]. The three layers are combined to form a crossbar array in the memristor [40]. High-density memristor crossbar array is effective in memory and information processing [41]. In this structure, the two metal electrodes at both ends are stimulated by potentiation pulse (P-pulse) or depression pulse (D-pulse). These pulses contribute to increase memristor conductances acting as a bio-synaptic connection strength (i.e., weight), or decrease conductances [42]. It acts as same as the weight-optimization in the CNN models. It may help improve the accuracy of the CNN models through the optimally updated conductance values of memristors [43].

### *C. Overall Learning Process of M-CNNs and CNNs*

Fig. 3 presents the overall learning process of the CNNs and M-CNNs. In Fig. 3(a), the CNNs describe to obtain the weighted sum of the inputs ($x_1 - x_n$), and the M-CNNs also show to obtain that the weighted sum of the inputs as shown in Fig. 3(b).

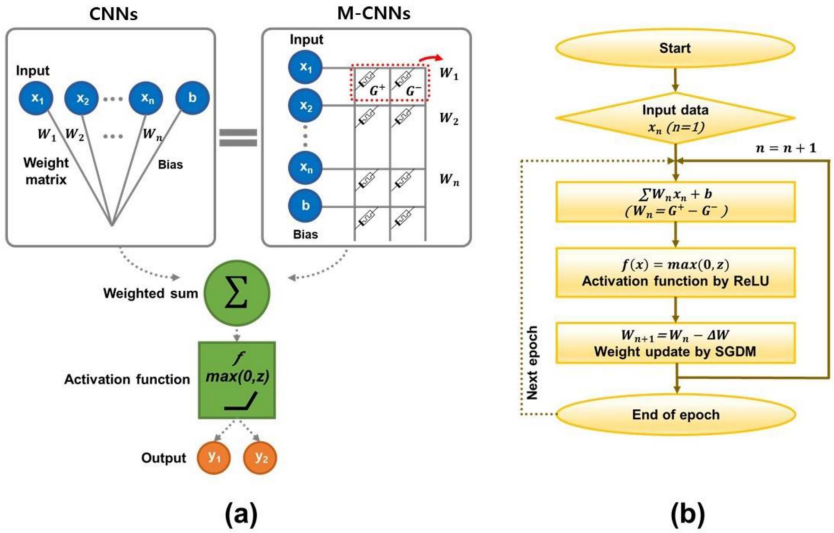


Fig. 3. Schematics of the M-CNNs and CNNs. (a) The process to yield output by calculating the weighted sum for CNNs in the left panel and M-CNNs in the right panel. In two models, the inputs ($x_n$) are multiplied by each weight. Unlike CNNs, $G^+$ and $G^-$ must be additionally subtracted to calculate each weight of the memristors in the M-CNNs. Memristor's conductance is expressed by weight at each cross-point in the crossbar array structure. Thereafter, both models are calculated as max$(0,\ z)$ using ReLU, one of the most popular activation functions. Therefore, the output values ($y$) are calculated as the weighted sum $f(\Sigma\ W_n\ x_n + b)$ and the current weights ($W_n$) are updated to the next weights ($W_{n+1}$). (b) Flow chart for the process of M-CNNs in (a).

Additionally, we added a bias ($b$), which adjusts the output value to each weighted sum. The learning process of the M-CNNs is identical to that of the CNNs. Both CNNs and M-CNNs should update their weights after forward passes of data through the neural network. The weights can be adjusted to reduce the difference between the actual and predicted classification results for subsequent forward passes [44]. Unlike CNNs, M-CNNs have to additionally calculate the difference between $G^+$ and $G^-$ to obtain the current weights ($W_1 - W_n$). Eventually, we only replaced weights of the M-CNN with memristor conductance values. To convert the memristor's conductances into weights, we calculated the difference between the positive conductance and negative conductance changes ($w\ = G^+\ - G^-$) as a weight. $G^+$ and $G^-$ represent the increased and decreased conductances in the potentiation process and the depression process by applying the number of pulses, respectively. The desired conductance of each memristor can then be translated into a predetermined number of electrical pulses for each device using the SGDM algorithm. The weights were updated as follows:

$$V_t = V_{t-1} - \alpha\nabla E\left(V_{t-1}\right) + \gamma\left(V_{t-1} - V_{t-1} - 1\right) \quad (1)$$

$$\Delta w = w - V_t \quad (2)$$

where, $V$and $t$ are the moving average of the gradients and the number of repetitions in the neural network, respectively. $\alpha$ is the learning rate and $\nabla E(V_{t-1})$ is the loss function. $\gamma$ determines the proportion of the previous gradient step in the present gradient step.

Successively, the activation function is performed in common on both CNNs and M-CNNs using the rectified linear unit (ReLU). The ReLU function is one of the most commonly used activation functions in neural networks [45]. It is defined as $\max\ (0, z)$, where $z$ are the values obtained by the weighted sum of CNNs and M-CNNs. In this process, the weight update by the SGDM is continuously generated and the current weight ($W_n$) is updated to the next weight ($W_{n+1}$). In summary, the output values ($y$) are calculated using the ReLU for the weighted sum $f(\Sigma\ W_n x_n + b\ )$ and then $W_n$ is updated to $W_{n+1}$. Thus, we can acquire the binary classification results between the control and stress groups.

### D. Neural Network Architectures

M-CNN and CNN have the same network configuration, except that the memristor conductances are used as the weight values in M-CNN. We designed the overall neural network architecture for stress image recognition between the control and stress groups. There are five layers composed of two convolution layers, two ReLU layers, two max-pooling layers, one fully connected layer, and a softmax output layer. These layers were divided into the roles of feature learning and classification as illustrated in Fig. 4. The input for the first layer is a $28(\text{width})$ x $28(\text{height})$ x $3(\text{color channels})$ scale image. This image that passed through the first convolutional layer consists of $28 * 28 * 128$ dimensions. Filters, also known as kernels, are responsible for detecting image features. All convolution kernels are $3 * 3$ with stride 1. Furthermore, all max-pooling kernels are $2 * 2$ with stride 2. Stride means the movement interval of the filter, which adjusts the output size. The second convolutional layer is $14 * 14 * 256$. Finally, a fully connected layer has $12544$ output units, and we can obtain binary classification results through the softmax output layer, which represents the probability of belonging to either class. It is a typical CNN structure in memristor-related fields [10]. We conducted a literature review on hyperparameter tuning and adopted an approach used by a previous researcher. Following the work of Wu et al. [50], we

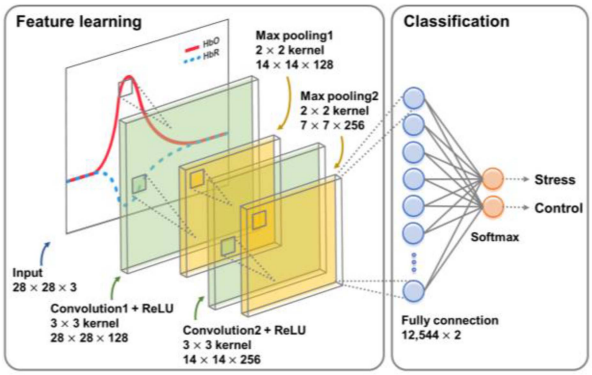


Fig. 4. Neural network architecture. This network has two convolution layers, two ReLU layers, two max-pooling layers, and one fully connected layer, followed by a softmax output layer. We define a kernel as a function to detect image features. All convolution kernels are 3∗3 with stride 1; all max-pooling kernels are 2∗2 with stride 2. The fully connected layer has 12544 output units.

fine-tuned certain hyperparameters, such as the learning rate (0.0001), momentum, maximum epochs (100), and mini-batch size (64), to attain the highest accuracy in the proposed model. Subsequently, we tested by 10-fold cross-validation to avoid overfitting known as learning biases caused by the classifier's excessive dependency on training data. We divided them into the ratio of 9 train sets and 1 test sets for the cross-validation. Each classifier model was tested 30 times (10 fold x 3 runs = 30) and then the mean classification accuracy and a standard error of the mean (SEM) were calculated to estimate the variability of the accuracies. All the processes were conducted in a personal computer (Intel(R) Core(TM) i5-10400 CPU; Microsoft Windows 10 Home OS; NVIDIA GeForce GTX 1070 Ti).

### E. Criteria for Evaluating the Reliability of Calculated Results

Confusion matrix has been known as one of the best ways to demonstrate the reliability of calculated accuracy results derived from classifier models based on the combination of four matrices: TP, TN, FP, and FN. We also calculated the precision, recall, accuracy, and F-Score from confusion matrix values. They have a range of 0 to 100, and the closer they are to 100, the better the reliability of the result. Four-evaluation matrices can be calculated by the confusion matrix that indicates row (i.e., true label) and column (predicted label) by a classifier based on the test dataset. The four metrics are defined below. The precision can be defined by

$$Precision = \frac{TP}{TP + FP} \tag{3}$$

where, TP is the true-positive case, which judges the stress group as a stress group. FP is the false-positive case, which is the misjudgment of a control group as a stress group. Thus, precision means the ratio of actual true-positive cases to true-positive cases.

The recall refers to the ratio of true-positive cases predicted by the classifier to true-positive cases as follows.

$$Recall = \frac{TP}{TP + FN} \tag{4}$$

where, FN is the false-negative case. It is the misjudgment of a stress group as a control group.

The accuracy is the ratio of correctly predicted data among all data.

$$Accuracy = \frac{TP + TN}{TP + TN + FP + FN} \tag{5}$$

where, TN is the true-negative case. The control group was well determined as a control group.

Finally, F-Score is one of the indicators to determine how accurately the classifier distinguishes control groups or stress groups well, by using the trade-off relationship between precision and recall.

$$F - Score = 2 \times \frac{(Precision \times Recall)}{(Precision + Recall)} \tag{6}$$

### F. Statistical Analysis Using Two-Independent Sample t-Test

To compare variances of the accuracies calculated from M-CNNs and CNNs, we assessed the homogeneity of variance for the classification accuracy between the control and stress groups using the Levene's test [46]. Then, we used a two-independent sample t-test to evaluate between-group and between-model differences in the classification accuracy.

## III. Results

### A. Characteristics of Memristive Synaptic Devices

We investigated the characteristics of fabricated $Pr_{0.7}Ca_{0.3}MnO_3$ memristors to determine whether the conductance measured from the memristors can be used as a weight of the neural networks. Fig. 5(a) presents the typical memristor I-V curve measured from a memristor. This I-V curve has a hysteresis loop, which shows the genuine synaptic characteristics of memristors. Specifically, the current suddenly increases or decreases at the set or reset process in accordance with a set voltage of $-1.5$ V and a reset voltage of $+2.0$ V, respectively. The voltage values are determined depending on a cyclical voltage sweep. Similarly, Fig. 5(b) represents the potentiation and depression curves, which are measured from the $Pr_{0.7}Ca_{0.3}MnO_3$ memristor by applying 100 consecutive P-pulses of -0.892 V, 100 consecutive D-pulses of $+0.880$ V, with a duration of 0.1 $\mu s$. The P-pulses and the D-pulses are represented by the orange circles and the green circles, respectively. An optimal voltage range of P- or D-pulses can be estimated by using set and reset voltages to obtain high linearity of conductance. High linearity of conductance prevents abrupt current changes in memristors. The conductance variations are almost linearly increased or decreased depending on the P- or D-pulses. With these characteristics of the memristor, we can convert the conductances of the memristors into weights in the neural networks.

### B. Classification Accuracies Obtained From M-CNN and C-CNN

To enhance the classification accuracies between the control and stress groups, we used the brain imaging data converted from the hemodynamic responses of fNIRS. Fig. 6 presents the

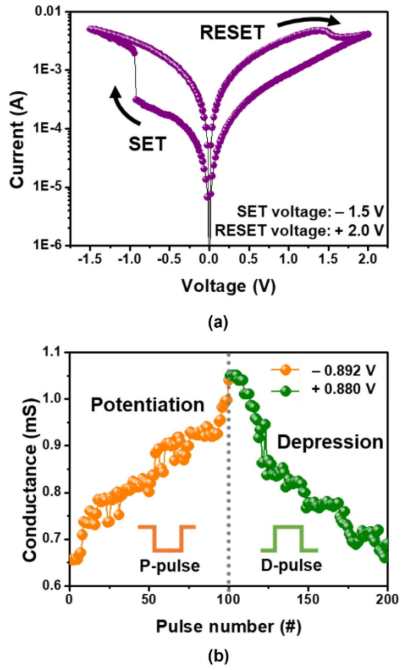


Fig. 5. Characteristics of fabricated $Pr_{0.7}Ca_{0.3}MnO_3$ memristors; (a) I-V loop with a set voltage of $-1.5\ V$ and a reset voltage of $+2.0\ V$ in accordance with voltage sweep. This I-V loop has a hysteresis shape, showing the genuine synaptic characteristics of memristors. (b) Potentiation and depression curves, which flexibly change and transmit signals in response to external stimuli. It is critical to obtain high linear conductance in the memristor to avoid abrupt changes in current. To obtain the high linearity of the conductances, 100 P-pulses ($-0.892\ V$) and duration ($1\ \mu s$) followed by 100 D-pulse ($+0.880\ V$) are applied. P-pulses are the orange circles and D-pulses refer to the green circles. It is possible to estimate the optimal voltage range of P- or D-pulse from the set and reset voltages. With these characteristics of memristors, we can obtain conductance, which can be used as a weight for neural networks.

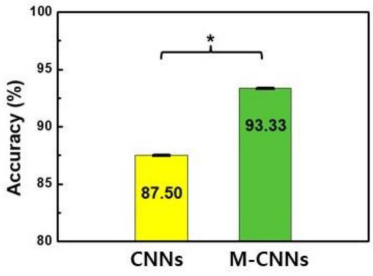


Fig. 6. Bar graphs of the averaged classification accuracy between CNNs (the conventional CNNs) and M-CNNs (memristor-based CNNs); The yellow bar represents the CNNs case, indicating accuracy and SEM ($87.50 \pm 0.02\%$) between control and stress groups. The green bar represents the M-CNNs, which obtained a high accuracy and SEM ($93.33 \pm 0.01\%$). This means that M-CNN has a 5.83% higher accuracy than C-CNN. We found a statistically significant difference between CNNs and M-CNNs ($t = 2.728;\ *p < 0.05$), indicating that the accuracy gap between the two models is large.

average accuracies by using the C-CNN and M-CNN models. The yellow bar represents to the classification accuracy using the C-CNN model and the green bar represents the classification accuracy using the M-CNN model. The error bar was calculated using the SEM to observe the variability of the accuracies. The average classification accuracies and SEMs were achieved to be $87.50 \pm 0.02\%$ and $93.33 \pm 0.01\%$ in the C-CNN and M-CNN, respectively. Moreover, we can statistically exhibit a significant difference in the accuracy between the proposed C-CNN and the M-CNN ($t = 2.728;\ *p < 0.05$). Our proposed M-CNN model is superior to the C-CNN model to classify stress states.

### C. Reliability Validations of Calculated Results Using Confusion Matrix

Fig. 7 presents the confusion matrix tables of the CNNs and M-CNNs. The columns in the confusion matrix corresponds to the "true label" of actual data, and the row corresponds to the "predicted label" forecasted from each model. Fig. 7(a) presents the indexing confusion matrix indicating the meaning of each cell i.e., TP, TN, FP, and FN. We can estimate each indicator through the match between the "true label" and "predicted label". Moreover, the green cells represent to be accurately classified as matrices such as TN and TP, but the pink cells are misclassified in the confusion matrix. The classification accuracy based on the ratio of the green to the pink cells indicates the precision and recall which are indicated by the light gray cells, and the final classification accuracy is represented by the dark gray cells. Fig. 7(b) and (c) represent the accuracies in the CNNs (87.50%) and the M-CNNs (93.33%), respectively. The M-CNNs show 5.83% higher accuracy than the CNNs. Furthermore, the CNNs exhibits a precision of 86.99%, a recall of 89.17%, and an F-Score of 88.00% using the confusion matrix by (3) to (6). Likewise, the M-CNNs show a precision of 93.33%, a recall of 93.33%, and an F-Score of 93.00%. All evaluation matrix values were calculated between 0 and 100, and the closer it is to 100, the higher is the reliability. Eventually, the accuracy results of both models are reliable and even indicate that the results from the M-CNNs are relatively more reliable than those of the CNNs.

## IV. Discussion

### A. Higher Classification Accuracy Between Control and Stress Groups in M-CNN Than CNN

Previous studies have proved that the existing CNN was more accurate than the CNN combined with memristors. According to Pan et al. [47], CNN models exhibited 3.44% higher classification accuracy than the M-CNN combined with $TiN/LiSiO_x/Pt$ memristor, and 1.88% higher classification accuracy than M-CNN combined with $TiN/HfO_2/Ti$. On the other hand, our findings are contrary to their findings. Our M-CNN (93.33%) obtained a higher classification accuracy than the CNNs (87.50%), as illustrated in Fig. 6. The M-CNN shows higher accuracy by 5.83% than the CNN as shown in Fig. 5(b), because their weights are updated linearly and symmetrically [10]. The appropriate weights are determined by linear conductances derived by P-pulse or D-pulse amplitude. To obtain highly linear conductance, we continuously increased or decreased the amplitudes of P-pulse or D-pulse until the curvatures of potentiation and depression curves in Fig. 5(b) should be close to zero [48]. Here, the nearly zero curvatures refer to the points at which the slopes of both curves are the largest. In this study, the M-CNN model

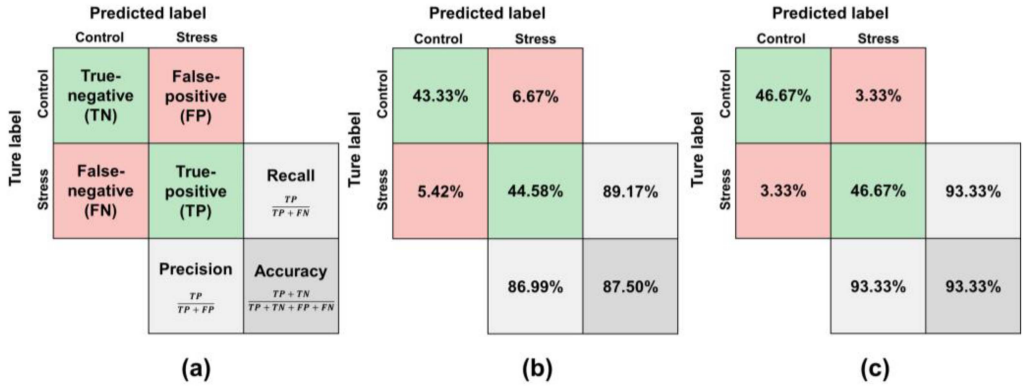


Fig. 7. Confusion matrix proving the reliability of the classification accuracy results between the control group and the stress group. These confusion matrices show the averaged accuracy results among the 30 tests attempted to show a distinct difference in the accuracy between CNNs and M-CNNs. The column refers to the 'True label' of actual data, whereas the row is the 'Predicted label' forecasted by classifier models. Depending on the matching of these two labels, evaluation matrices such as precision, recall, and accuracy can be estimated by TP, FP, FN, and TN. (a) Example table explaining each cell within the confusion matrix. TP judged the stress group as a stress group and FP misjudged the control group as a stress group. FN also misjudged the stress group as a control group. Finally, TN determined the control group as a control group. The green cells are the correctly classified result, and the pink cells show the misclassification results. The light gray cells are precision and recall, and the dark gray cells represent the final classification accuracy. (b) and (c) present the confusion matrices of the CNNs and M-CNNs, respectively. To classify between the control and stress groups, we finally achieved precision (86.99%), recall (89.17%), accuracy (87.50%) at (b) and precision (93.33%), recall (93.33%), accuracy (93.33%) at (c). We found that our proposed M-CNNs had 5.83% higher accuracy than the CNNs, and both models satisfied the reliability of the results.

used the weights obtained from stimulating the memristors by P-pulses (-0.892 V) or D-pulses (+0.880 V) whose curvature is close to zero, and therefore we could obtain the optimized weight values. It also limits the weight range within $\pm 1$ [47]. A previous study has demonstrated that if long-term potentiation exhibits sufficient linearity, high accuracy can be attained irrespective of the values of long-term depression [49]. Therefore, we propose the M-CNN model to classify stress states compared to the existing C-CNN.

### B. Classification Accuracies Obtained From M-DenseNet and C-DenseNet

To guarantee a fair and reliable comparison, we additionally compared our proposed model to the DenseNet model, which is known as state-of-the-art neural network model [50]. To compare the accuracy of DenseNet model, we divided it into C-DenseNet and M-DenseNet models. We calculated the binary classification accuracy between the control and stress groups. The hyperparameters were set such as mini-batch size (64), max epochs (100), the learning rate (0.0001), and growth rate (32) [51]. It was the same setting as the M-CNN, except for the growth rate that exists only on the DenseNet. As a result, we achieved the classification accuracies of $90.00 \pm 0.01\%$ and $92.38 \pm 0.02\%$ for the C-DenseNet and the M-DenseNet, respectively. It shows that the M-DenseNet has higher accuracy by 2.38% than the C-DenseNet. We also confirmed that all the calculated results are reliable by using the confusion matrix; the C-DenseNet shows precision (91.00%), recall (90.00%), and F-Score (90.00%). Similarly, the M-DenseNet represents precision (91.00%), recall (93.00%), and F-Score (92.00%).

Eventually, the neural network models combined with memristors show higher classification accuracy than the traditional models because of updating weights linearly and symmetrically [10]. Moreover, we confirmed that the CNN model is more accurate than the latest DenseNet model. Because the DenseNet model tends to extract similar features as the hierarchy deepens, which affects accuracy [52]. Our study shows that the CNN model is better than the DenseNet model in terms of the classification accuracy.

### C. M-CNN Applications Utilizing Various Biosensor Data

Most of the memristor-based neural network studies mainly classify handwritten digit datasets based on MNIST. This is well illustrated in Table I. However, several studies have recently attempted to utilize memristor-based neural networks for biological datasets, such as electrocardiogram (ECG), electroencephalogram (EEG), and so on. Zhang et al. [53] developed an epilepsy detection system based on a CNN and memristor to predict epilepsy with EEG data [54]. The system achieved a detecting accuracy of 98.46%, indicating its excellent performance in epilepsy detection. Another study reported that an accuracy of 93.60% was obtained in 4-class ECG classification tasks by using a multi-layer deep integrative spiking neural network [55]. Recently, Ham et al. [56] developed an artificial neural network (ANN) that can detect heart diseases using actual bio-signals, but the classification accuracy was only 70.00%. Through a fusion of computed tomography and MRI images, Zhu et al. implemented a memristive pulse coupled neural network to help diagnose brain diseases by performing medical image processing [57]. In line with this research trend, our study also performed the stress classification of brain images based on fNIRS through M-CNN and consequently achieved an accuracy of 93.33%. Thus, we proved that our proposed M-CNN model is a good candidate for the classification of fNIRS-based stress imaging data for the first time.

TABLE I
COMPARISON OF THE MNIST'S DIGIT RECOGNITION RESULTS ISSUED OVER THE PAST 4 YEARS USING MEMRISTIVE NEURAL NETWORKS

| Authors | Issued years | Memristor structure | Neural networks | Accuracy (%) |
|---|---|---|---|---|
| Hu *et al.* | 2018 | Ta/ $HfO_2$ /Pd | M-CNN | 89.90 |
| Xu *et al.* | 2018 | Cr/Au/SWCNTs/$Al_2O_3$/polyimide | M-CNN | 90.00 |
| Li *et al.* | 2018 | Ta/$HfO_2$/Pt | M-CNN | 91.71 |
| Wen *et al.* | 2018 | Pt/$TiO_2$/Pt | M-CNN | 92.46 |
| Wang *et al.* | 2018 | Au/$HfO_2$/$SiO_2$ | M-CNN | 90.00 |
| Bayat *et al.* | 2018 | Pt/$Al_2O_3$/$TiO_{2-x}$/Ti/Pt | M-CNN | 81.40 |
| Sun *et al.* | 2019 | Ti/$AlO_x$/$TaO_x$/Pt | M-CNN | 93.54 |
| Krestinskaya *et al.* | 2019 | $WO_x$ | M-CNN | 93.00 |
| Nguyen *et al.* | 2019 | Pt/$LaAlO_3$/Nb-doped $SrTiO_3$ | M-CNN | 92.00 |
| Chen *et al.* | 2020 | Ti/$HfO_2$ /TiN | M-CNN | 92.79 |
| Pan *et al.* | 2020 | TiN/$LiSiO_x$/Pt | M-CNN | 95.25 |
| Li *et al.* | 2020 | Ta/$TaO_x$/Pt | M-CNN | 95.30 |
| Truong *et al.* | 2021 | Pt/$LaAlO_3$/Nb-doped $SrTiO_3$ | M-CNN | 95.00 |
| Jang *et al.* | 2021 | W/$HfO_2$/TiN | M-CNN | 90.70 |
| Jang *et al.* | 2021 | W/$HfO_2$/TiN | M-CNN | 90.00 |
| Huang *et al.* | 2021 | Pt/$HfO_2$:Cu/Cu | M-CNN | 93.43 |
| ***Our proposed model*** | ***2022*** | ***Pt/$Pr_{0.7}Ca_{0.3}MnO_3$/TiN*** | ***M-CNN*** | ***96.16*** |

It has obtained high classification accuracy ranging from 81.40% to 95.30%. However, we obtained the highest classification accuracy of 96.16%, compared with other results. These studies are currently considered mainstream in the study of memristor-based neural networks.

### *D. Reproducibility of M-CNN and M-DenseNet Models for Other Dataset Types*

M-CNN can improve the classification accuracy compared to CNN as illustrated in Fig. 6. Moreover, this classification accuracy is guaranteed by the confusion matrix values. Despite this systematic process, there is a possibility that the classification results are not reproducible for other datasets. We selected the model-specific datasets MNIST and Merchandise (Merch) to check the reproducibility. We used the same processes as the main simulation to calculate the classification accuracy of each dataset. In Fig. 8(a), CNN indicates the accuracies in the Stress dataset (87.50%) and MNIST (95.32%). Moreover, M-CNN presents the Stress dataset (93.33%) and MNIST (96.16%), respectively. Similarly, C-Densenet shows the accuracies in the Stress dataset (90.00%) and Merch set (90.95%). M-DenseNet also shows the Stress dataset (92.38%) and Merch (93.57%), respectively, in Fig. 8(b). All the accuracy results are reliable by the confusion matrix in each dataset. Hence, M-CNN and M-DenseNet models always exhibit higher classification accuracy for each dataset, indicating that M-CNN and M-DenseNet models produce reproducible results for all datasets used in this study.

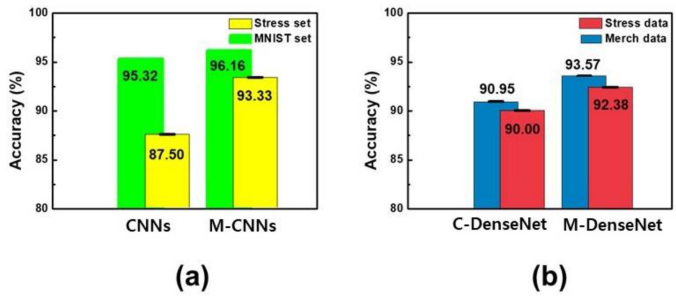


Fig. 8. Bar graphs of the averaged classification accuracy to test the reproducibility in various dataset types using (a) CNN and (b) DenseNet. In (a), the yellow bars represent accuracies of CNNs and M-CNNs based on the stress dataset, and the green bars refer to those of the two models based on the MNIST dataset. The CNNs achieved accuracy and SEM ($87.50 \pm 0.02\%$) in the stress dataset and ($95.32 \pm 0.00\%$) in the MNIST datasets. On the other hand, M-CNNs obtained classification results of ($93.33 \pm 0.01\%$) in the stress dataset and ($96.16 \pm 0.00\%$) in MNIST datasets. We found that there is an accuracy differences between CNNs and M-CNNs in Stress data ($t = 2.728$; $*p < 0.05$) and MNIST data ($t = 5.176$; $***p < 0.001$). Similarly, the red bars represent the accuracies of C-DenseNet and M-DenseNet based on the stress dataset, and the blue bars refer to those of the two models based on the Merch dataset in (b). The C-DenseNet shows accuracy and SEM ($90.00 \pm 0.01\%$) in the stress dataset and ($90.95 \pm 0.01\%$) in the Merch datasets. On the other hand, M-DenseNet shows the classification results of ($92.38 \pm 0.02\%$) in the stress dataset and ($93.57 \pm 0.01\%$) in the Merch datasets. However, they found no difference in accuracy between C-DenseNet and D-DenseNet in both stress data and Merch data. As a result, the memristor based models outperform under all the conditions, and they are reproducible on any dataset.

### *E. Reliability of Classification Accuracy Results Estimated By Confusion Matrix*

In this study, we investigated the confusion matrix to satisfy the reliability criteria of the classification accuracy results obtained by the M-CNN and CNN models. The use of the confusion matrix is justifiable as it has been extensively employed in artificial intelligence research, including the evaluation of CNN models, to assess the reliability of model performance. [58], [59], [60], [61].

However, this process is likely to be overlooked in most memristor-based neural network studies [62], [63], [64]. For example, a recent study classified the MNIST datasets using a tantalum oxide memristor-based ANN and obtained an accuracy of 89.08% [65]. They used the confusion matrix to investigate the reliability of their accuracy results, but was insufficient because they did not show the detailed evaluation matrices, such as precision, recall, and F-Score [65]. Another study also performed a validation process for reliability considering various image sizes based on MNIST, however, the evaluation matrix was not presented [66]. Except for them, most studies did not go through a validation process using a confusion matrix [67], [68]. The confusion matrix can calculate matrices such as precision, recall, accuracy, and F-Score. Therefore, we conducted a validation process using a confusion matrix in our classification results. All of the models used in this study produced reliable results.

## V. Conclusion

We proposed the M-CNN model that can classify stress states and then demonstrate its excellent classification performances compared with the existing CNN model. We used the publicly available stress datasets that were collected from our previous study. We first classified stress states, which achieved higher accuracy of M-CNN (93.33%) than that of CNN (87.50%). Unlike prior studies, we verified the reliability criteria using the confusion matrix including precision, recall, and F-Score in terms of the classification accuracy results of the two models. These findings are the same as those of DenseNet. However, it proved higher accuracy to CNN than DenseNet. Moreover, we found that the M-CNN/DenseNet models provided reproducible results regardless of the dataset types. Thus, the M-CNN model is suitable for improving the classification accuracy between the control and stress groups with high reliability as well as reproducible outcomes. Therefore, this study can help implement and optimize M-CNN incorporating hardware-based memristors and software-based CNNs to improve the classification accuracy of stress states.

## References


[1] J. von Neumann, "The principles of large-scale computing machines," *Ann. Hist. Comput.*, vol. 3, no. 3, pp. 263–273, Jul.–Sep. 1981.

[2] J. C. Kao, S. D. Stavisky, D. Sussillo, P. Nuyujukian, and K. V. Shenoy, "Information systems opportunities in brain–machine interface decoders," *Proc. IEEE*, vol. 102, no. 5, pp. 666–682, May 2014.

[3] D. Ielmini, D. Sharma, S. Lavizzari, and A. L. Lacaita, "Reliability impact of chalcogenide-structure relaxation in phase-change memory (PCM) cells—Part I: Experimental study," *IEEE Trans. Electron Devices*, vol. 56, no. 5, pp. 1070–1077, May 2009.

[4] B. C. Lee, E. Ipek, O. Mutlu, and D. Burger, "Architecting phase change memory as a scalable dram alternative," in *Proc. 36th Annu. Int. Symp. Comput. Architecture*, 2009, pp. 2–13.

[5] M. Kund et al., "Conductive bridging RAM (CBRAM): An emerging non-volatile memory technology scalable to sub 20nm," in *Proc. IEEE Int. Electron Devices Meeting, Tech. Dig.*, 2005, pp. 754–757.

[6] C. Song et al., "Tempo-spatial compressed sensing of organ-on-a-chip for pervasive health," *IEEE J. Biomed. Health Inform.*, vol. 22, no. 2, pp. 325–334, Mar. 2018.

[7] D. Kuzum, S. Yu, and H. P. Wong, "Synaptic electronics: Materials, devices and applications," *Nanotechnology*, vol. 24, no. 38, 2013, Art. no. 382001.

[8] A. S. Demirkol, I. Messaris, A. Ascoli, and R. Tetzlaff, "Pattern formation in an M-CNN structure utilizing a locally active NbO memristor," in *Memristor Computing Systems*. Berlin, Germany: Springer, 2022, pp. 79–101.

[9] A. Slavova and E. Litsyn, "Edge-of-chaos in CNN models with memristor synapses," in *Memristor Computing Systems*. Berlin, Germany: Springer, 2022, pp. 3–20.

[10] P. Yao et al., "Fully hardware-implemented memristor convolutional neural network," *Nature*, vol. 577, no. 7792, pp. 641–646, 2020.

[11] L. Huang et al., "Memristor based binary convolutional neural network architecture with configurable neurons," *Front. Neurosci.*, vol. 15, 2021, Art. no. 639526.

[12] H.-Y. Zhang, C. E. Stevenson, T.-P. Jung, and L.-W. Ko, "Stress-induced effects in resting EEG spectra predict the performance of SSVEP-based BCI," *IEEE Trans. Neural Syst. Rehabil. Eng.*, vol. 28, no. 8, pp. 1771–1780, Aug. 2020.

[13] E. Smets, W. De Raedt, and C. Van Hoof, "Into the wild: The challenges of physiological stress detection in laboratory and ambulatory settings," *IEEE J. Biomed. Health Inform.*, vol. 23, no. 2, pp. 463–473, Mar. 2019.

[14] R. Fu et al., "Symmetric convolutional and adversarial neural network enables improved mental stress classification from EEG," *IEEE Trans. Neural Syst. Rehabil. Eng.*, vol. 30, pp. 1384–1400, 2022.

[15] L. G. Hernández, O. M. Mozos, J. M. Ferrández, and J. M. J. F. Antelis, "EEG-based detection of braking intention under different car driving conditions," *Front. Neuroinform.*, vol. 12, 2018, Art. no. 29.

[16] S. Kim, C. Du, P. Sheridan, W. Ma, S. Choi, and W. D. Lu, "Experimental demonstration of a second-order memristor and its ability to biorealistically implement synaptic plasticity," *Nano Lett.*, vol. 15, no. 3, pp. 2203–2211, 2015.

[17] Z. Q. Wang, H. Y. Xu, X. H. Li, H. Yu, Y. C. Liu, and X. J. Zhu, "Synaptic learning and memory functions achieved using oxygen ion migration/diffusion in an amorphous InGaZnO memristor," *Adv. Funct. Mater.*, vol. 22, no. 13, pp. 2759–2765, 2012.

[18] G. Liu et al., "Organic biomimicking memristor for information storage and processing applications," *Adv. Electron. Mater.*, vol. 2, no. 2, 2016, Art. no. 1500298.

[19] S. Bak, J. Shin, and J. Jeong, "Subdividing stress groups into eustress and distress groups using laterality index calculated from brain hemodynamic response," *Biosensors*, vol. 12, no. 1, 2022, Art. no. 33.

[20] R. Wang, Y. Hao, Q. Yu, M. Chen, I. Humar, and G. Fortino, "Depression analysis and recognition based on functional near-infrared spectroscopy," *IEEE J. Biomed. Health Inform.*, vol. 25, no. 12, pp. 4289–4299, Dec. 2021.

[21] R. Zimmermann et al., "Detection of motor execution using a hybrid fNIRS-biosignal BCI: A feasibility study," *J. Neuroengineering Rehabil.*, vol. 10, no. 1, pp. 1–15, 2013.

[22] H. Tsunashima and K. Yanagisawa, "Measurement of brain function of car driver using functional near-infrared spectroscopy (fNIRS)," *Comput. Intell. Neurosci.*, vol. 2009, pp. 1–12, 2009.

[23] U. Asgher et al., "Enhanced accuracy for multiclass mental workload detection using long short-term memory for brain–computer interface," *Front. Neurosci.*, vol. 14, 2020, Art. no. 584.

[24] J. Wang, T. Grant, S. V. Gursoy, B. Geng, and L. Hirshfield, "Taking a deeper look at the brain: Predicting visual perceptual and working memory load from high-density fNIRS data," *IEEE J. Biomed. Health Inform.*, vol. 26, no. 5, pp. 2308–2319, May 2022.

[25] T. K. K. Ho, J. Gwak, C. M. Park, and J.-I. Song, "Discrimination of mental workload levels from multi-channel fNIRS using deep leaning-based approaches," *IEEE Access*, vol. 7, pp. 24392–24403, 2019.

[26] U. Asgher, K. Khalil, Y. Ayaz, R. Ahmad, and M. J. Khan, "Classification of mental workload (MWL) using support vector machines (SVM) and convolutional neural networks (CNN)," in *Proc. IEEE 3rd Int. Conf. Comput., Math. Eng. Technol.*, 2020, pp. 1–6.

[27] J.-H. Lee, J. R. Anaraki, C. W. Ahn, and J. An, "Efficient classification system based on Fuzzy–Rough feature selection and multitree genetic programming for intension pattern recognition using brain signal," *Expert Syst. Appl.*, vol. 42, no. 3, pp. 1644–1651, 2015.

[28] D. T. Delpy, M. Cope, P. van der Zee, S. Arridge, S. Wray, and J. Wyatt, "Estimation of optical pathlength through tissue from direct time of flight measurement," *Phys. Med. Biol.*, vol. 33, no. 12, 1988, Art. no. 1433.

[29] H. Sato et al., "A NIRS–fMRI investigation of prefrontal cortex activity during a working memory task," *Neuroimage*, vol. 83, pp. 158–173, 2013.

[30] S. M. Shahid, S. Ko, and S. Kwon, "Real-time abnormality detection and classification in diesel engine operations with convolutional neural network," *Expert Syst. Appl.*, vol. 192, 2021, Art. no. 116233.

[31] Y. Pyo, J.-U. Woo, H.-G. Hwang, S. Nahm, and J. Jeong, "Effect of oxygen vacancy on the conduction modulation linearity and classification accuracy of $Pr_{0.7}Ca_{0.3}MnO_3$ memristor," *Nanomaterials*, vol. 11, no. 10, 2021, Art. no. 2684.
[32] S. Yu, Y. Wu, R. Jeyasingh, D. Kuzum, and H.-S. P. Wong, "An electronic synapse device based on metal oxide resistive switching memory for neuromorphic computation," *IEEE Trans. Electron Devices*, vol. 58, no. 8, pp. 2729–2737, Aug. 2011.
[33] Y. Wang, G. Wang, Y. Shen, and H. H.-C. Iu, "A memristor neural network using synaptic plasticity and its associative memory," *Circuits, Syst., Signal Process.*, vol. 39, pp. 3496–3511, 2020.
[34] A. Thomas, "Memristor-based neural networks," *J. Phys. D: Appl. Phys.*, vol. 46, no. 9, 2013, Art. no. 093001.
[35] D. Negrov, I. Karandashev, V. Shakirov, Y. Matveyev, W. Dunin-Barkowski, and A. Zenkevich, "An approximate backpropagation learning rule for memristor based neural networks using synaptic plasticity," *Neurocomputing*, vol. 237, pp. 193–199, 2017.
[36] X. Zhang et al., "Emulating short-term and long-term plasticity of bio-synapse based on Cu/a-Si/Pt memristor," *IEEE Electron Device Lett.*, vol. 38, no. 9, pp. 1208–1211, Sep. 2017.
[37] L. F. Abbott and S. B. Nelson, "Synaptic plasticity: Taming the beast," *Nature Neurosci.*, vol. 3, no. 11, pp. 1178–1183, 2000.
[38] A. J. Watt and N. S. Desai, "Homeostatic plasticity and STDP: Keeping a neuron's cool in a fluctuating world," *Front. Synaptic Neurosci.*, vol. 2, 2010, Art. no. 5.
[39] Z. Shen et al., "Advances of RRAM devices: Resistive switching mechanisms, materials and bionic synaptic application," *Nanomaterials*, vol. 10, no. 8, 2020, Art. no. 1437.
[40] J. Chen, L. Wang, and S. Duan, "A mixed-kernel, variable-dimension memristive CNN for electronic nose recognition," *Neurocomputing*, vol. 461, pp. 129–136, 2021.
[41] V. M. Ho, J.-A. Lee, and K. C. Martin, "The cell biology of synaptic plasticity," *Science*, vol. 334, no. 6056, pp. 623–628, 2011.
[42] H. Zhang et al., "Research progress of biomimetic memristor flexible synapse," *Coatings*, vol. 12, no. 1, 2021, Art. no. 21.
[43] M. Hu, H. Li, Y. Chen, Q. Wu, G. S. Rose, and R. W. Linderman, "Memristor crossbar-based neuromorphic computing system: A case study," *IEEE Trans. Neural Netw. Learn. Syst.*, vol. 25, no. 10, pp. 1864–1878, Oct. 2014.
[44] H. A. Ghiassirad, M. A. Shoorehdeli, and F. Farivar, "Application of constrained learning in making deep networks more transparent, regularized, and biologically plausible," *Eng. Appl. Artif. Intell.*, vol. 85, pp. 421–428, 2019.
[45] A. Beke and T. Kumbasar, "Learning with type-2 fuzzy activation functions to improve the performance of deep neural networks," *Eng. Appl. Artif. Intell.*, vol. 85, pp. 372–384, 2019.
[46] G. Walker and J. Shostak, *Common Statistical Methods for Clinical Research With SAS Examples*. Cary, NC, USA: SAS Inst., 2010.
[47] W.-Q. Pan et al., "Strategies to improve the accuracy of memristor-based convolutional neural networks," *IEEE Trans. Electron Devices*, vol. 67, no. 3, pp. 895–901, Mar. 2020.
[48] S. Seo et al., "Artificial optic-neural synapse for colored and color-mixed pattern recognition," *Nature Commun.*, vol. 9, no. 1, pp. 1–8, 2018.
[49] O. Bichler, M. Suri, D. Querlioz, D. Vuillaume, B. DeSalvo, and C. Gamrat, "Visual pattern extraction using energy-efficient '2-PCM synapse' neuromorphic architecture," *IEEE Trans. Electron Devices*, vol. 59, no. 8, pp. 2206–2214, Aug. 2012.
[50] A. M. Roy, J. J. C. Bhaduri, and E. I. Agriculture, "Real-time growth stage detection model for high degree of occultation using DenseNet-fused YOLOv4," *Comput. Electron. Agriculture*, vol. 193, 2022, Art. no. 106694.
[51] G. Huang, Z. Liu, L. Van Der Maaten, and K. Q. Weinberger, "Densely connected convolutional networks," in *Proc. IEEE Conf. Comput. Vis. Pattern Recognit.*, 2017, pp. 2261–2269.
[52] H. Gao, T. Zhen, and Z. Li, "Detection of wheat unsound kernels based on improved ResNet," *IEEE Access*, vol. 10, pp. 20092–20101, 2022.
[53] J. Zhang et al., "EEG signal epilepsy detection system based on convolutional neural network and memristor array," in *Proc. IEEE 4th Int. Conf. Electron. Technol.*, 2021, pp. 851–855.
[54] Y. Li, "A novel statistical algorithm for multiclass EEG signal classification," *Eng. Appl. Artif. Intell.*, vol. 34, pp. 154–167, 2014.
[55] J. Jiang et al., "MSPAN: A memristive spike-based computing engine with adaptive neuron for edge arrhythmia detection," *Front. Neurosci.*, vol. 15, 2021, Art. no. 761127.
[56] S. Ham et al., "One-dimensional organic artificial multi-synapses enabling electronic textile neural network for wearable neuromorphic applications," *Sci. Adv.*, vol. 6, no. 28, 2020, Art. no. eaba1178.
[57] S. Zhu, L. Wang, and S. Duan, "Memristive pulse coupled neural network with applications in medical image processing," *Neurocomputing*, vol. 227, pp. 149–157, 2017.
[58] X.-X. Niu and C. Y. Suen, "A novel hybrid CNN–SVM classifier for recognizing handwritten digits," *Pattern Recognit.*, vol. 45, no. 4, pp. 1318–1325, 2012.
[59] L. Eren, T. Ince, and S. Kiranyaz, "A generic intelligent bearing fault diagnosis system using compact adaptive 1D CNN classifier," *J. Signal Process. Syst.*, vol. 91, pp. 179–189, 2019.
[60] S. Meister, M. Wermes, J. Stueve, and R. M. Groves, "Cross-evaluation of a parallel operating SVM–CNN classifier for reliable internal decision-making processes in composite inspection," *J. Manuf. Syst.*, vol. 60, pp. 620–639, 2021.
[61] C. Silva, J. Weber, and B. Belloni, "Segmentation and detection of cattle branding images using CNN and SVM classification," *Adv. Distrib. Comput. Artif. Intell. J.*, vol. 8, 2019, Art. no. 19.
[62] R. A. Sporea, I. S. Pesch, E. Bestelink, O. de Sagazan, and A. Mehonic, "Multimodal transistors as ReLU activation functions in physical neural network classifiers," *Scientific Rep.*, vol. 12, no. 1, Univ. of Surrey, p. 670, 2022.
[63] S. Wen et al., "CKFO: Convolution kernel first operated algorithm with applications in memristor-based convolutional neural network," *IEEE Trans. Comput.-Aided Des. Integr. Circuits Syst.*, vol. 40, no. 8, pp. 1640–1647, Aug. 2021.
[64] A. Alhudhaif, K. Polat, and O. Karaman, "Determination of COVID-19 pneumonia based on generalized convolutional neural network model from chest X-ray images," *Expert Syst. Appl.*, vol. 180, 2021, Art. no. 115141.
[65] S. Choi et al., "A self-rectifying TaO y/nanoporous TaO x memristor synaptic array for learning and energy-efficient neuromorphic systems," *NPG Asia Mater.*, vol. 10, no. 12, pp. 1097–1106, 2018.
[66] F. Aguirre, S. Pazos, F. Palumbo, N. Gomez, E. Miranda, and J. Suñé, "Line resistance impact in memristor-based multi layer perceptron for pattern recognition," in *Proc. IEEE 12th Latin Amer. Symp. Circuits Syst.*, 2021, pp. 1–4.
[67] M. Hu et al., "Memristor-based analog computation and neural network classification with a dot product engine," *Adv. Mater.*, vol. 30, no. 9, 2018, Art. no. 1705914.
[68] L. Huang et al., "Memristor based binary convolutional neural network architecture with configurable neurons," *Front. Neurosci.*, vol. 15, 2021, Art. no. 639526.